
The Pobei Cu-Ni and Fe ore deposits in NW China are comagmatic evolution products: evidence from ore microscopy, zircon U-Pb chronology and geochemistry

Y.G. LIU^{1,2,3} W.Y. LI¹ X.B. LÜ^{2*} Y.H. HUO⁴ B. ZHANG⁵

¹Key Laboratory for the Study of Focused Magmatism and Giant Ore Deposits, Ministry of Land and Resources, Xi'an Center of Geological Survey

Liu E-mail: ltdzgj_2006@126.com

²Institute of Geological Survey, China University of Geosciences, Wuhan

388 Lumo Road, Hongshan District, Wuhan 430074, China. Lü Email: luxb@cug.edu.cn

³College of Earth Science and Resources, Chang'an University

⁴School of Earth Science, Lanzhou University

E-mail: huoyh14@lzu.edu.cn

⁵Key Laboratory of Orogenic Belt and Crustal Evolution, Peking University

E-mail: zhangbo5015@foxmail.com

*Corresponding author

| A B S T R A C T |

The Pobei mafic-ultramafic complex in northwestern China comprises magmatic Cu-Ni sulfide ore deposits coexisting with Fe-Ti oxide deposits. The Poshi, Poyi, and Podong ultramafic intrusions host the Cu-Ni ore. The ultramafic intrusions experienced four stages during its formation. The intrusion sequence was as follows: dunite, hornblende-peridotite, wehrlite and pyroxenite. The wall rock of the ultramafic intrusions is the gabbro intrusion in the southwestern of the Pobei complex. The Xiaochangshan magmatic deposit outcrops in the magnetite-mineralized gabbro in the northeastern part of the Pobei complex. The main emplacement events related to the mineralization in the Pobei complex, are the magnetite-mineralized gabbro related to the Xiaochangshan Fe deposit, the gabbro intrusion associated to the Poyi, Poshi and Podong Cu-Ni deposits, and the ultramafic intrusions that host Cu-Ni deposits (Poyi and Poshi). The U-Pb age of the magnetite-mineralized gabbro is 276 ± 1.7 Ma, which is similar to that of the Pobei mafic intrusions. The $\epsilon_{\text{Hf}}(t)$ value of zircon in the magnetite-mineralized gabbro is almost the same as that of the gabbro around the Poyi and Poshi Cu-Ni deposits, indicating that the rocks related to Cu-Ni and magnetite deposits probably originated from the same parental magma. There is a trend of crystallization differentiation evolution in the Harker diagram from the dunite in the Cu-Ni deposit to the magnetite-mineralized gabbro. The monosulfide solid solution fractional crystallization was weak in Pobei; thus, the Pd/Ir values were only influenced by the crystallization of silicate minerals. The more complete the magma evolution is, the greater is the Pd/Ir ratio. The Pd/Ir values of dunite, the lithofacies containing sulfide (including hornblende peridotite, wehrlite, and pyroxenite) in the Poyi Cu-Ni deposit, magnetite-mineralized gabbro, and massive magnetite, are 8.55, 12.18, 12.26, and 18.14, respectively. Thus, the massive magnetite was probably the latest product in the evolution of the Pobei mafic-ultramafic intrusions. We infer that the Cu-Ni sulfide and Fe-Ti

oxide ores in the Pobei area were products of a cogenetic magma at different evolutionary stages; at the late stage, the magma became iron enriched through crystallization differentiation. The magma differentiation occurred in a deep staging magma chamber emplaced in the upper magma chamber. Earlier crystallized olivine with some interstitial sulfides gathered at the bottom of the staging magma chamber because of its greater density. That is to say, the ultramafic magma hosting the Cu-Ni sulfide formed at the bottom of the staging magma chamber, while the magnetite-mineralized gabbro was in the upper part. However, the magnetite-mineralized gabbro injected into the upper magma chamber first and the ultramafic lithofacies containing the olivine and the interstitial Cu-Ni sulfides were subsequently emplaced in the upper magma chamber as crystal mush.

KEYWORDS | Magmatic Cu-Ni sulfide deposit. Xiaochangshan Fe deposit. Crystallization differentiation. Magnetite-mineralized gabbro. Beishan. Early Permian.

INTRODUCTION

The Pobei mafic-ultramafic complex is unique because of the coexistence of magmatic Cu-Ni sulfide ore and Fe-Ti oxide deposits. The symbiosis of magmatic sulfide deposits and magmatic titanium iron oxide ore (including magnetite, ilmenite, and titanomagnetite) is visible in some parts of the world (Wang *et al.*, 2010). For example, not only chromium and Platinum Group Elements (PGE) but also magnetite ore outcrops are found in the Bushevelid complex (Cawthorn and Molyneux, 1986). The Xinjie layered intrusion in the Panxi area of China contains both vanadic-titanomagnetite and copper-nickel-platinum. The upper part has two layers of vanadium-titanium magnetite, while the lower part has four layers of Cu-Ni-Pt sulfide ore (Li *et al.*, 2006a; Zhu *et al.*, 2010; Zhong *et al.*, 2011). The Xiangshan intrusion in the eastern Tianshan area of China hosts both Ti-Fe and Cu-Ni sulfide mineralization (Wang *et al.*, 2006, 2009; Xiao *et al.*, 2010).

There are two hypotheses explaining the coexistence of the magmatic sulfide ore deposit and the Fe-Ti oxide deposit. One is that the formation of Fe-Ti oxide ore occurred later than that of the sulfide; the Cu-Ni sulfide ore and the Fe-Ti oxide ore were products of a cogenetic magma at different evolutionary stages; and the liquids were iron enriched through fractionation at the late stage in the layered intrusions (Scoon and Mitchell, 1994; Wang *et al.*, 2006, 2009; Xia, 2009; Xiao *et al.*, 2010; Jiang, 2014). The other hypothesis argues that the Fe-Ti oxide ore was formed earlier than the sulfides, while periodic magma recharge and the continuous mixing of resident and replenishing ferropicritic magma led to the crystallization of minor chromite and Cr-bearing magnetite and, thereafter, to relatively abundant Fe-Ti oxides, with the resultant S saturation giving rise to PGE-enriched sulfide droplets (Zhu *et al.*, 2010; Zhong *et al.*, 2011).

Based on field observations, geochronology, major and trace element geochemistry, and PGE geochemistry, we discuss the petrogenetic relationships between Cu-

Ni sulfide and magnetite deposits and the mineralization process in the Pobei complex. A deep understanding of the relationship between the magmatic Cu-Ni sulfide ore and Fe-Ti oxide deposits will help the exploration of mafic-ultramafic intrusions, especially the metallogenic types.

GEOLOGIC SETTING

Early Permian mafic-ultramafic intrusions discovered at the northeastern margin of the Tarim Basin in Xinjiang in northwestern China (Fig. 1), host economic magmatic sulfide deposits. This made Xinjiang the second most important district of nickel resources in China (Mao *et al.*, 2008; Qin *et al.*, 2011; Han *et al.*, 2013; Yang *et al.*, 2014).

The Tarim Basin is the largest sedimentary basin in China (Fig. 1B). According to recent geological mapping, drill core logging, and seismic data, the Permian ultramafic-mafic rocks of the the Large Igneous Province (LIP) in the Tarim Basin, form a NE-SW-trending zone across the basin, with an outcrop area of approximately 250,000km² (Fig. 1B; Jia, 1997). The Permian igneous units are dominated by basalts, with some peridotites, gabbros, basaltic andesites, and dolerites.

Basalt is mainly distributed in the eastern and southern part of the Bachu area, and the Early Permian Tajilitag V-Ti-Fe deposit is located in the southeast (Fig. 1B) (Li *et al.*, 2001; Zhang *et al.*, 2008a). Early Permian basalt has also been found in the Liuyuan and Pobei areas in Beishan, along the northeastern margin of Tarim (Jiang *et al.*, 2007; Xiao, 2004).

The Cu-Ni deposits along the northeastern margin of the Tarim Basin are mainly distributed in three areas (Fig. 1C): Beishan (Pobei), central Tianshan, and eastern Tianshan (Han *et al.*, 2004; Zhou *et al.*, 2004; Jiang *et al.*, 2006; Chai *et al.*, 2008; Zhang *et al.*, 2008b; Han *et al.*, 2010; Qin *et al.*, 2011; Zhang *et al.*, 2011; Tang *et al.*, 2012; Zhao *et al.*, 2015; Liu *et al.*, 2015, 2016).

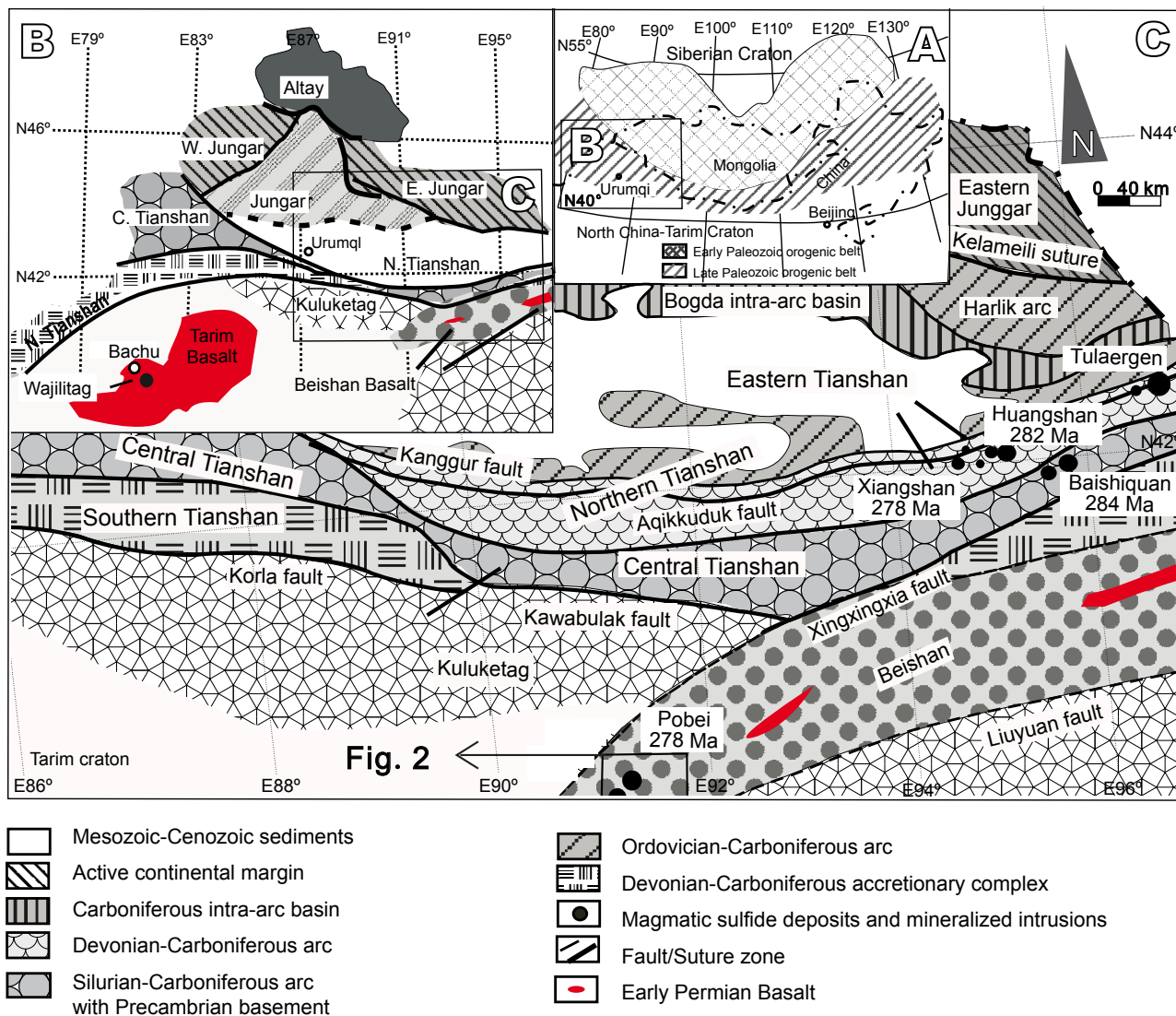


FIGURE 1. Tectonic units and distribution of magmatic deposits and Early Permian basalts in northern Xinjiang, northwestern China (modified after BGMRXUAR, 1993; Xiao *et al.*, 2004), and age resources (Qin *et al.*, 2002; Mao *et al.*, 2003; Wu *et al.*, 2005; Li *et al.*, 2006b; Xiao *et al.*, 2010; Jiang *et al.*, 2012).

The Cu-Ni deposits related to the Early Permian mafic-ultramafic complexes in eastern Tianshan include the Huangshandong, Tulargen, Huangshanxi, Hulu, and Xianshan deposits (Fig. 1C). The surrounding rocks are mainly Middle Ordovician and Carboniferous strata (Dong, 2005).

Central Tianshan was formed from a Precambrian block containing both the Tianyu and Baishiquan Cu-Ni deposits (Fig. 1C). The surrounding rocks of these deposits comprise Paleoproterozoic and Mesoproterozoic strata, which are mainly composed of mica quartz schist, gneiss, and migmatite, with ages in the range of 997Ma–1829Ma (Dong, 2005).

The Beishan (Pobei) area is generally considered to be the rift (Xiao, 2004; Su *et al.*, 2011) in which the Poyi and

Poshi Cu-Ni deposits formed related to mafic-ultramafic intrusions (Fig. 1C). The surrounding rocks of these intrusions include Paleoproterozoic quartz-biotite schist (2203 ± 74 Ma), Mesoproterozoic gneissic biotite-plagioclase granite (1311Ma), mica quartz schist, and marble (Xiao, 2004).

The intergrowth of the fault sag and fault uplift in the Beishan region separates the pre-Permian sedimentary sequences (BGMRXUAR, 1993; Qin *et al.*, 2011); the discovery of Permian bimodal igneous rocks in the Pobei area (Su *et al.*, 2011; Yang, 2011) supports the fact that the Beishan region, in which the Pobei Cu-Ni-Fe deposit is located, is a Permian rift (Xiao, 2004). The Beishan Rift Zone is composed of Precambrian crystalline basement, mainly Paleoproterozoic rocks, overlaid by sedimentary

rocks (Xiao, 2004). The rift zone is separated from the Kruktag Block by the Xingxingxia fault in the west and from the Dunhuang Block by the Liuyuan fault in the east (Fig. 1).

The exposed rocks in the Beishan area are mainly part of the Paleoproterozoic Beishan group, the Mesoproterozoic Gudongjing group, the Lower Paleozoic Cambrian Shuangyingshan Formation, the Silurian Tushenbulake Formation, the Carboniferous Hongliuyuan Formation, the Shibanshan Formation, the Shengliquan Formation, the Permian Hongliuhe Formation, the Luotugou Formation, the Paleogene Taoshuyuan Formation, and the Neogene Kuquan Formation (Xiao, 2004).

The Pobei mafic-ultramafic complex is approximately 35km in length and 8km in width. The mafic-ultramafic intrusions exhibit close relationships with regional faults (Fig. 2). The Baidiwa-Yunihe fault has a long-term effect on the distribution of the Pobei mafic-ultramafic intrusions and iron-copper-nickel ore deposits.

GEOLOGY OF THE POBEI Cu-Ni AND XIAOCHANGSHAN FE DEPOSITS

The Pobei complex is mainly composed of three mafic intrusions: gabbro, magnetite-mineralized gabbro, and leucocratic gabbro, from southwest to northeast (Fig. 2). The wall rock of the Poshi, Poyi, and Podong ultramafic rocks

which host the Cu-Ni ore, comprises gabbro intrusions; the Xiaochangshan Fe deposit outcrops in the southern part of the magnetite-mineralized gabbro intrusion (Fig. 2). In the field, the gabbro cross-cutting the magnetite-mineralized gabbro (Fig. 3) indicates that the gabbro intrusion around the Poyi and Poshi Cu-Ni deposits was emplaced later than the magnetite-mineralized gabbro.

The Poyi multiple ultramafic intrusion experienced four stages during its formation. The intrusion sequence was as follows: dunite, hornblende-peridotite, wehrlite, and pyroxenite (Liu, 2015). The Poshi ultramafic intrusion has these four lithofacies together with troctolite. The Cu-Ni ore bodies (Ni% higher than 0.4%) only exists in the hornblende-peridotite in both the Poyi and Poshi deposits.. The contact between the peridotite unit and the gabbro intrusions show a clear intrusive relationship. Moreover, gabbro xenoliths of several meters can be observed in the peridotite (Yang, 2011).

Therefore, there were three main emplacement events related to the mineralization in the Pobei complex, from early to late: the magnetite-mineralized gabbro related to the Xiaochangshan Fe deposit, the gabbro intrusion associated to the Poyi and Poshi Cu-Ni deposits, and the ultramafic intrusions that host Cu-Ni deposits (Poyi and Poshi).

The magnetite-mineralized gabbro is black (Fig. 4). Clinopyroxene (Cpx) accounts for 35%–40% and is

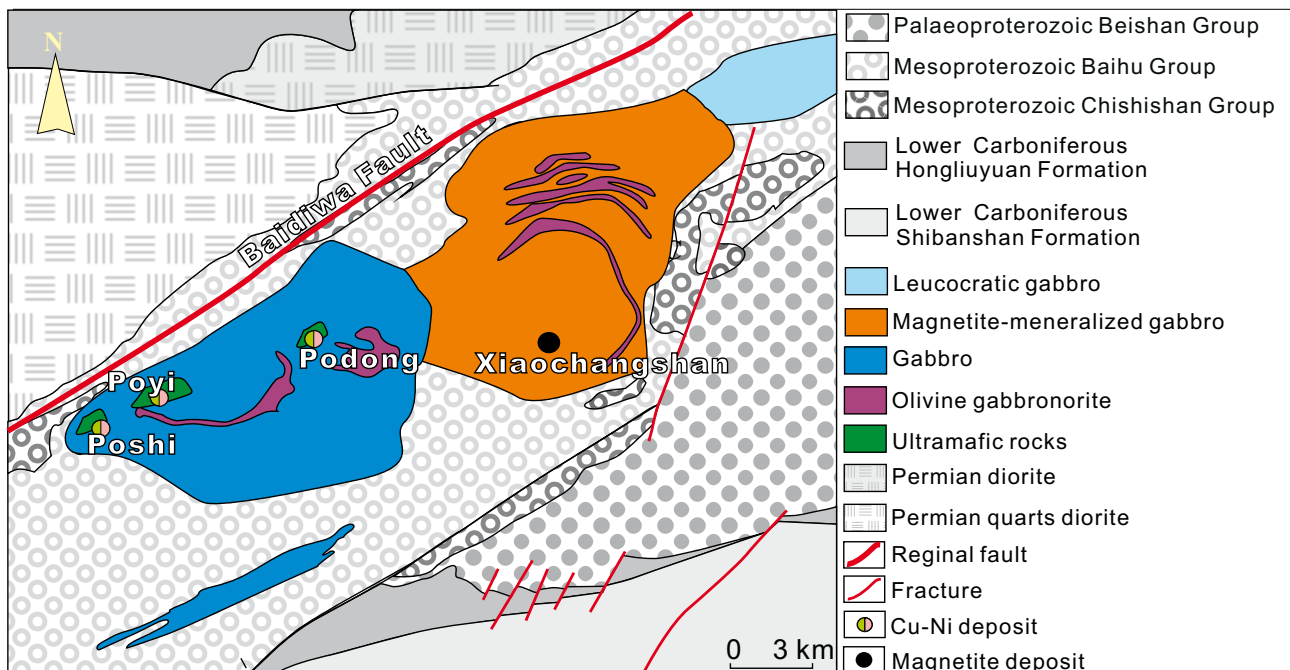


FIGURE 2. Geologic map of the Pobei mafic-ultramafic complex.

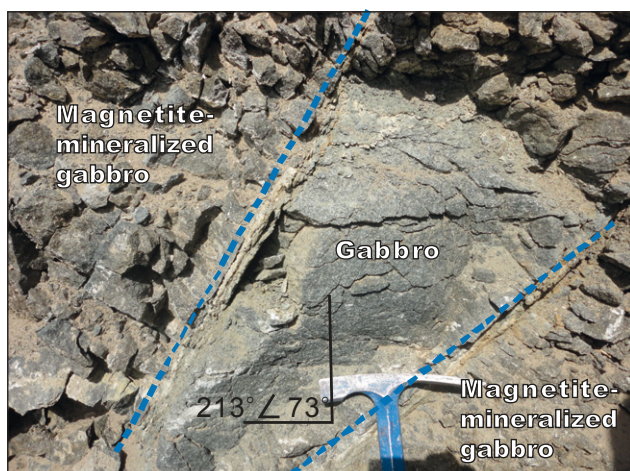


FIGURE 3. Gabbro around the Poyi and Poshi Cu-Ni deposits cross-cutting the magnetite-mineralized gabbro.

euhedral to subhedral, with a particle size of approximately 0.5x1mm; plagioclase (Pl) accounts for 50%–55% and is euhedral to subhedral, with a particle size of approximately 0.5x1mm; and accounting for 2%–4% magnetite (Mt) also exists in intergranular clinopyroxene and plagioclase (Fig. 4); therefore, Mt crystallized later than Cpx and Pl. The body of the Xiaochangshan magnetite ore is mainly located around the contact of the magnetite-mineralized gabbro and marble (Fig. 5). The ore mineral is magnetite, and ilmenite is rare.

ANALYTICAL METHODS

Major and rare elements of 11 magnetite-mineralized gabbro samples were analyzed at ALS Chemex (Guangzhou) Co. Ltd using ME-XRF26 and ME-MS81

methods, respectively. The analysis method for the loss of ignition was ME-GRA05.

The platinum group elements (PGEs) concentrations in 6 magnetite-mineralized gabbro samples and 2 Massive magnetite samples were determined at the Institute of Geochemistry of the State Key Laboratory of Ore Deposit Geochemistry in Guiyang, China, by Inductively Coupled Plasma-Mass Spectrometry (ICP-MS) coupled with a modified Carius tube isotope dilution method (Qi *et al.*, 2007).

U-Pb dating and trace-element analysis of zircon from the magnetite-mineralized gabbro were conducted synchronously by Laser Ablation-Inductively Coupled Plasma-Mass Spectrometry (LA-ICP-MS) at the State Key Laboratory of Geological Processes and Mineral Resources of the China University of Geosciences in Wuhan. Detailed operating conditions for the laser ablation system and the ICP-MS instrument and data reduction are described in Hu *et al.* (2008, 2012b) and Liu *et al.* (2008, 2010). The preferred U-Th-Pb isotopic ratios used for the standard Zircon 91500 are from Wiedenbeck *et al.* (1995). The uncertainty of the preferred values for the external standard 91500 was propagated to the ultimate results. Concordia diagrams and weighted mean calculations were made using Isoplot/Ex_v.3 (Ludwig, 2003). The preferred values of element concentrations for the USGS reference glasses were taken from the GeoReM database. (<http://georem.mpch-mainz.gwdg.de/>).

In situ Hf isotope ratio analysis of zircon was conducted using a Neptune Plus MC-ICP-MS (Thermo Fisher Scientific, Germany) in combination with a Geolas 2005 excimer ArF laser ablation system (Lambda Physik, Göttingen, Germany) at the State Key Laboratory



FIGURE 4. Characteristics of the magnetite-mineralized gabbro in a hand specimen and under the optical microscope.

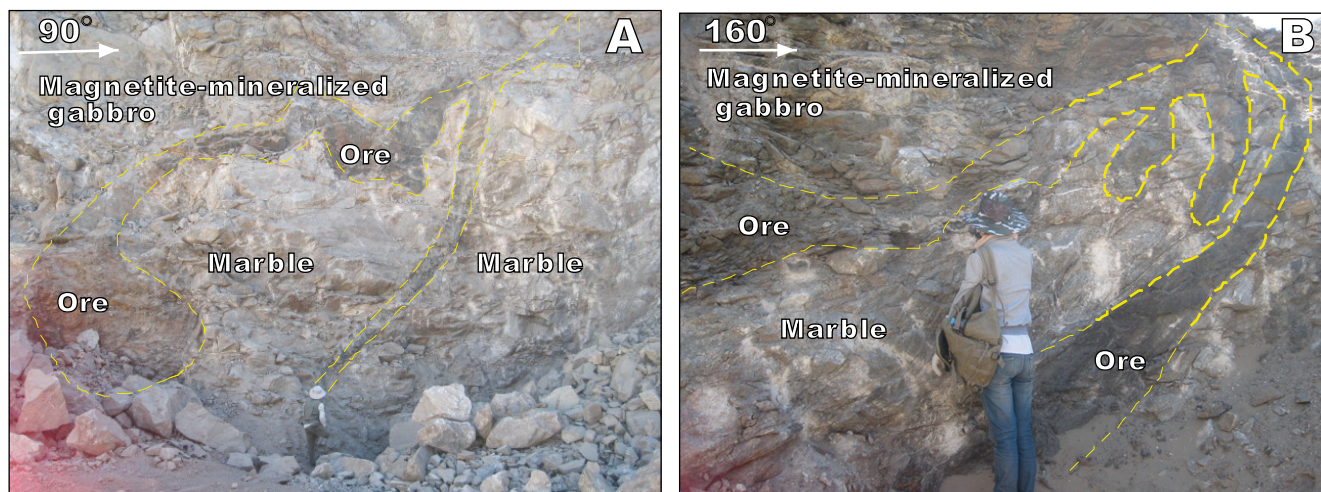


FIGURE 5. Relationship between the magnetite-mineralized gabbro and the magnetite ore body.

of Geological Processes and Mineral Resources of the China University of Geosciences in Wuhan. The detailed operating conditions are described in Hu *et al.* (2008, 2012a, b). The offline selection, integration of the signals, and mass bias calibrations were performed using ICP-MSDataCal (Liu *et al.*, 2010).

RESULTS

Geochronology

Zircon grains from all samples are transparent, mostly subhedral, and 50–150 μm in length. The internal structure of the selected zircon crystals from the magnetite-mineralized gabbro was studied with cathodoluminescence images (Fig. 6). Some of the grains exhibit concentric zoning, and others are structureless. The analytical results of the selected zircon crystals are listed in Table I (see Electronic Appendix at www.geologica-acta.com). The concordia plots of the analyses are shown in Figure 7. The U, Th, and Pb contents of the zircons vary from 196–1348 ppm, 112–947 ppm and 32–264 ppm, respectively, and the Th/U ratios are ~ 0.46 –0.82. All analyses give concordant U-Pb ages within analytical errors (Fig. 7), yielding a concordia age of $276 \pm 1.7 \text{ Ma}$ (MSWD=0.2) for the magnetite-mineralized gabbro.

Lutetium-Hafnium (Lu-Hf) isotopes

The Lu-Hf isotopes of the selected zircon crystals from the magnetite-mineralized gabbro are listed in Table II. The calculated $\epsilon\text{Hf}(t)$ values of these zircon crystals range from 4.0 to 6.1, and is 5.3 on average. While, the $\epsilon\text{Hf}(t)$ of the zircon crystals of the Pobei gabbro enclosing the Poyi and

Poshi Cu-Ni deposit ranges from -0.8 to 5.3, with 3.2 on average (Su *et al.*, 2011); thus, the magnetite-mineralized gabbro has a $\epsilon\text{Hf}(t)$ of zircon close to that of the Pobei gabbro around the Poyi and Poshi Cu-Ni deposits.

Major and Rare Earth Elements (REEs)

The concentrations of major and Rare Earth Elements (REEs) in the magnetite-mineralized gabbros are listed in Table III. The magnetite-mineralized gabbros contain 47.6%–55.8% SiO_2 , 15.2%–21.3% Al_2O_3 , 3.2%–10.9% MgO , 0.10%–0.45% MnO , 5.85%–16.26% Fe_2O_3 (total), 5.07%–12.95% CaO , 1.77%–3.97% Na_2O , 0.67%–2.79% TiO_2 , 0.20%–1.1% K_2O , 0.01%–1.26 P_2O_5 , 0.02%–0.07% V_2O_5 , and 29.19–194.9 ppm REEs.

Platinum Group Elements (PGEs)

The concentrations of PGEs in the magnetite-mineralized gabbro and massive magnetite ores are listed in Table IV. The magnetite-mineralized gabbro and magnetite ores have extremely low PGE concentrations (0.01–0.05 ppb Ir, 0.015–0.036 ppb Ru, 0.007–0.023 ppb Rh, 0.119–0.292 ppb Pt and 0.165–0.540 ppb Pd) and show left-leaning primitive mantle-normalized PGE patterns (Fig. 8). The ΣPGE content of the magnetite ores ranges between 0.644 and 0.746 ppb and is 0.695 on average, whereas that of the magnetite-mineralized gabbro is 0.4–0.69, with a mean value of 0.49. Both the magnetite-mineralized gabbro and magnetite ores have negative Ru anomalies in the primitive mantle-normalized PGE diagrams (Fig. 8) relative to primitive mantle concentrations (Barnes and Maier, 1999). The Pd/Ir ratio of the magnetite ores is 18.14, which is higher than that of the magnetite-mineralized gabbro.

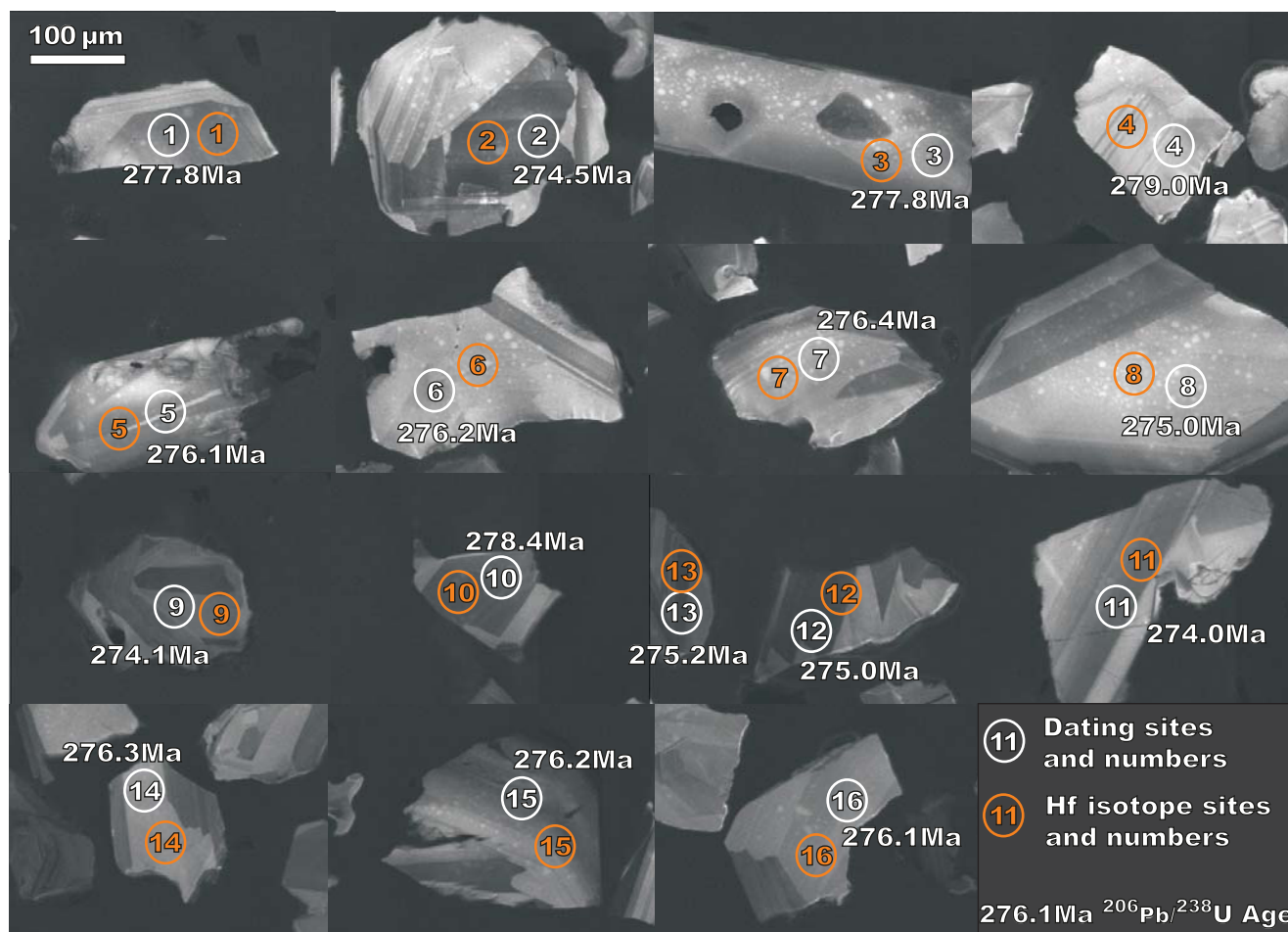


FIGURE 6. Cathodoluminescence images of selected zircon crystals of the magnetite-mineralized gabbro.

DISCUSSION

The U-Pb age of the magnetite-mineralized gabbro is 276 ± 1.7 Ma ($n=16$, MSWD=0.2; Fig. 7). The U-Pb ages of the zircon crystals separated from the gabbro intrusions, which formed the wallrock of the Poshi, Poyi, and Podong ultramafic rocks, where the Cu-Ni ores exist, are 274 ± 4 and 278 ± 2 Ma (Jiang *et al.*, 2006; Li *et al.*, 2006c). The fact that these two types of rock show the same age indicates that the rocks hosting the Cu-Ni and magnetite ore deposits probably originated from the same parental magma.

The average $\epsilon_{\text{Hf}}(t)$ value of the zircons from the magnetite-mineralized gabbro and the Pobei gabbro around the Poyi and Poshi Cu-Ni ore deposits is 5.3 and 3.2, respectively, which indicate that they probably have the same origin. We have also calculated the degree of contamination of the surrounding rocks using the two-endmember isotope-mixing model (Fig. 9). The surrounding rocks of the gabbros are the Mesoproterozoic Baihu Group (Fig. 2) which is mainly composed of

gneiss. So we chose the Mesoproterozoic gneiss with 8.85ppm Hf and $\epsilon_{\text{Hf}}(t=276\text{Ma})$ of -16.2 (He *et al.*, 2015, calculated from $\epsilon_{\text{Hf}}(t=1409\text{Ma})=7.0$) as one of the endmembers. Based on the Sr-Nd isotopes and trace elements, Yang (2011) suggested that the Pobei mafic-ultramafic rocks may have been derived from a depleted mantle source. Therefore, we chose the depleted mantle as the endmember. The Hf content of the depleted mantle (Fig. 9) is 2.05ppm (Sun and McDonough, 1989), and the $\epsilon_{\text{Hf}}(t=276\text{Ma})$ of the depleted mantle is 19.4, roughly calculated from Salters and Stracke (2004) and Griffin *et al.* (2000). The other endmember comprises the Beishan Mesoproterozoic gneiss with 8.85ppm Hf and $\epsilon_{\text{Hf}}(t=276\text{Ma})$ of -16.2 (He *et al.*, 2015, calculated from $\epsilon_{\text{Hf}}(t=1409\text{Ma})=7.0$). The comparison of the $\epsilon_{\text{Hf}}(t)$ values with those of the depleted mantle and a potential contaminant, the Mesoproterozoic gneiss from Beishan (He *et al.*, 2015), reveals that 13% and 16% of contamination are permitted for the magnetite-mineralized gabbro and the gabbro around the Poyi and Poshi Cu-Ni deposits, respectively (Fig. 9). The degree

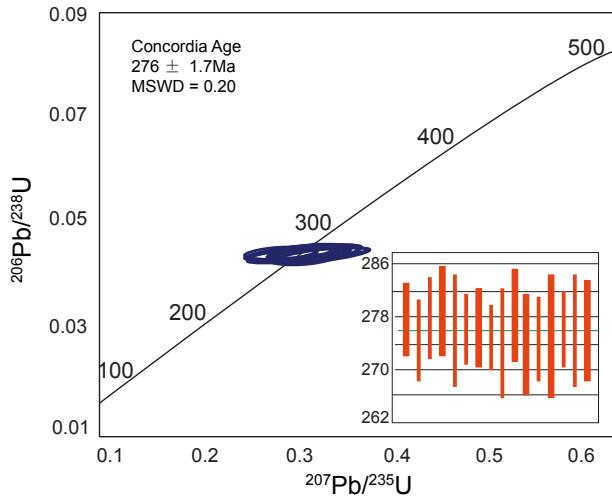


FIGURE 7. Zircon U-Pb isotope concordia plot for the magnetite-mineralized gabbro.

of contamination of these two types of gabbros with almost the same outcrop area is, in general, 15%. If the outcrop area of the two types of gabbros resulting from homologous evolution is roughly the same, the degree of contact with the surrounding rock is probably also the same; therefore, they may have a similar degree of crustal contamination.

To gain a better understanding of the relationship between the magnetite-mineralized gabbro and the mafic-ultramafic rocks related to the Cu-Ni ore deposits in the Pobei area, the major elements and REEs of mafic-ultramafic rocks related to Cu-Ni ore deposits in Pobei were compiled (Fig. 10).

The composition changes during the evolution of the magma because of the separation of crystals. The compositional change trends with MgO can reflect the

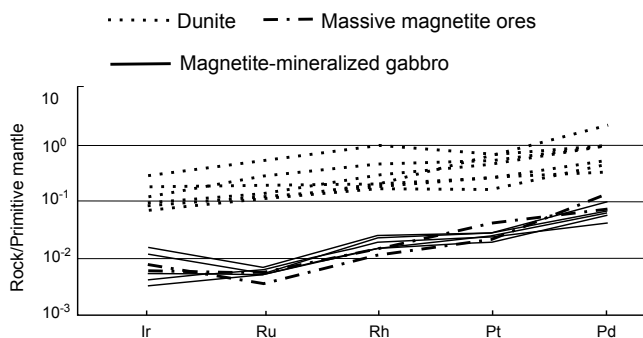


FIGURE 8. Primitive mantle-normalized PGE pattern of magnetite-mineralized gabbro, massive magnetite ores, and dunite in the Poyi deposit. Primitive mantle values are from Barnes and Maier (1999). The dunite data were taken from Liu *et al.* (2015).

process of crystallization differentiation (Bowen and Schairer, 1956). MgO is negatively related to SiO₂ and positively related to TFe₂O₃ (Fig. 10), indicating the crystallization differentiation of olivine. CaO and Al₂O₃ show a negative correlation with MgO (Fig. 10), indicating the crystallization differentiation of clinopyroxene. TiO₂ and MgO are negatively correlated (Fig. 10). A relationship between K₂O, P₂O₅, and MgO was not noted. The Harker diagrams of the Pobei mafic-ultramafic rocks, especially the relationships of SiO₂, TFe₂O₃, CaO, Al₂O₃, and MgO, reveal the crystallization differentiation evolutionary trend from the ultramafic rocks related to Cu-Ni deposits to the magnetite-mineralized gabbro related to the Xiaochangshan magmatic deposit. Although the Harker diagrams are not robust evidence to support the hypothesis of the same parental magma of the different intrusions, they at least do not contradict the crystallization differentiation evolutionary trend.

Because Mn, P, and REEs are not compatible with olivine and pyroxene during crystallization differentiation

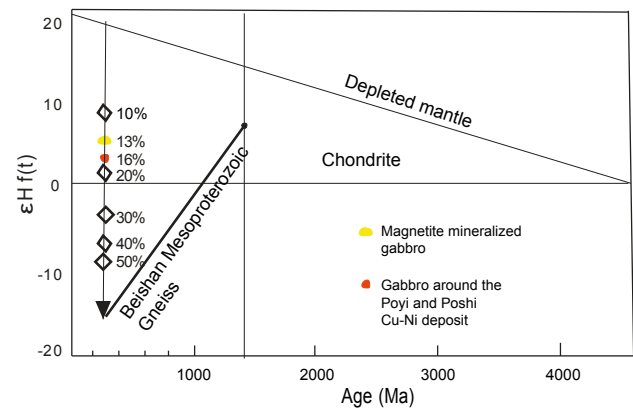


FIGURE 9. Quantitative simulation of the contamination degree of Paleoproterozoic rocks for two types of gabbro.

(Anderson and Greenland, 1969; Nagasawa *et al.*, 1980; Hirokazu *et al.*, 1984; Gaetani and Grove, 1997; Jones and Layne, 1997; Zack and Brumm, 1999; Adam and Green, 2006), they tend to be enriched in the residual phase. The magnetite-mineralized gabbro has the highest P, Mn, and REE contents (Fig. 10), which indicates that it is probably a later product of the magma evolution relative to the mafic-ultramafic rocks (*i.e.* dunite, hornblende-peridotite, wehrlite, and pyroxenite) that host the Cu-Ni deposits.

The PGEs, including Os, Ir, Ru, Rh, Pt, and Pd, have special chemical properties, leading to a different geochemical behavior compared to other trace elements. Therefore, the PGEs have a unique and irreplaceable geochemical tracer importance for the study of the

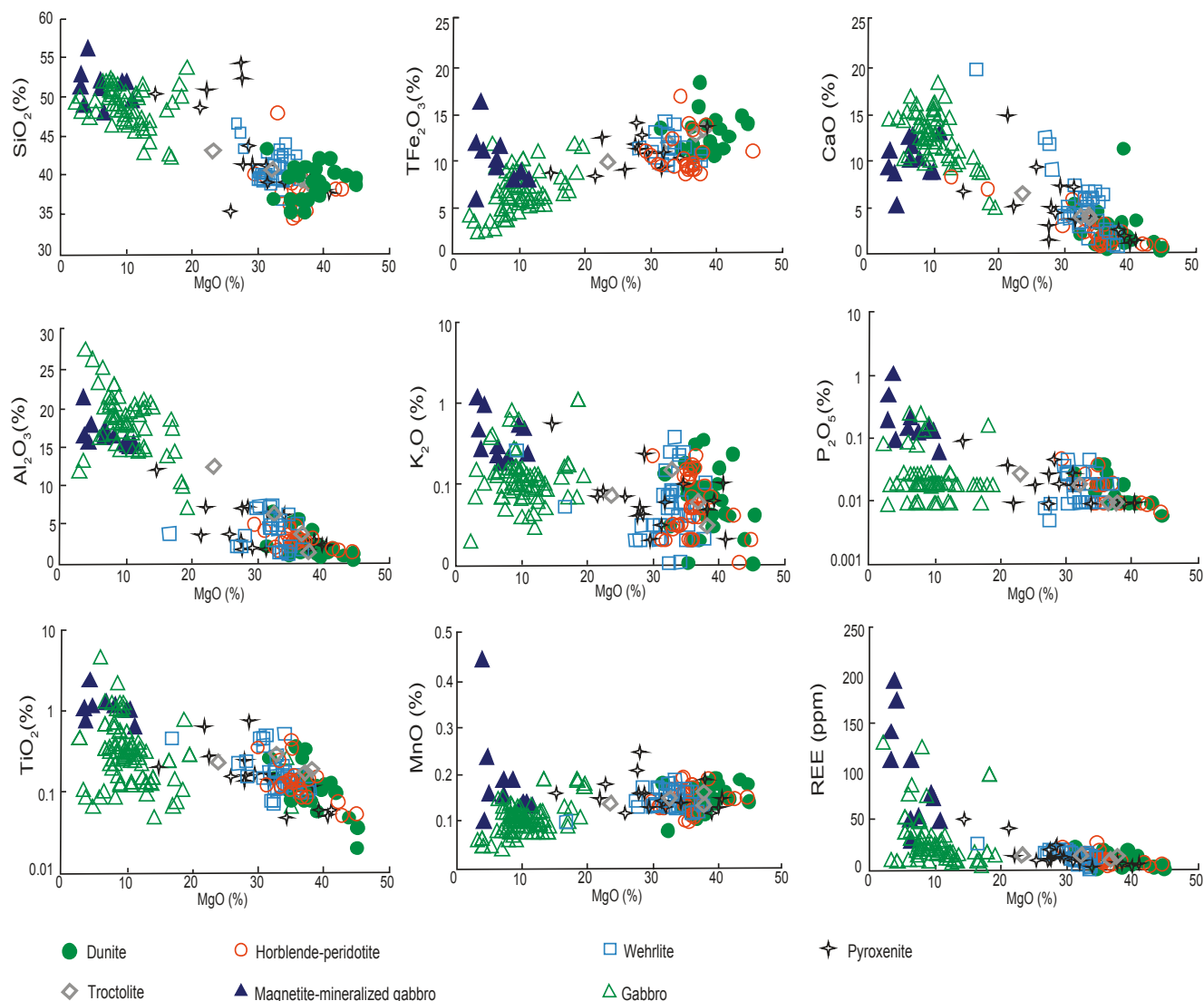


FIGURE 10. Harker diagrams of the Pobei mafic-ultramafic rocks (Jiang *et al.*, 2010; Ling, 2011; Liu, 2011; Yang, 2011; Guo *et al.*, 2012; Jiang *et al.*, 2012; Liu, 2015; magnetite-mineralized gabbro: data from this paper).

mantle-derived magma origin and evolution and the genesis of magmatic deposits (Qi *et al.*, 2007; Lorand *et al.*, 2008; Song *et al.*, 2009). Ruthenium is a compatible element during crystallization evolution (Capobianco *et al.*, 1994; Hill *et al.*, 2000; Puchtel and Humayun, 2001; Righter *et al.*, 2004) and thus will gradually be lost in the residual magma, magnetite-mineralized gabbro, and massive magnetite ores, which show a loss of Ru relative to dunite in the Poyi Cu-Ni ore deposits (Fig. 9), indicating that they may be later products compared to the Poyi ultramafic rocks (dunite). During the crystallization of the silicate minerals, Ir is compatible, while Pd is incompatible (Capobianco *et al.*, 1994; Hill *et al.*, 2000; Puchtel and Humayun, 2001; Righter *et al.*, 2004). Therefore, along with the crystallization of olivine,

chromite, and pyroxene, the Ir content will decrease, whereas the Pd content will increase in the residual phase, causing an increase in the Pd/Ir ratio. Therefore, the more complete the magma evolution is, the greater is the Pd/Ir. However, the Pd/Ir ratio can also be influenced by the sulfide fractional crystallization. Experimental studies indicate that the first phase to crystallize from a sulfide melt is a monosulfide solid solution (Mss; Naldrett *et al.*, 1967; Kullerud *et al.*, 1969; Misra and Flet, 1973, 1974). The Mss/sulfide liquid partition coefficient of Ir is 3.4–11, and that of Pd is 0.09–0.2 (Fleet *et al.*, 1993; Barnes *et al.*, 1997). If Ir were compatible during the fractionation of Mss in the rocks, Ir would show a negative correlation with Pd in the whole rock (Song *et al.*, 2008). It is clear that Ir has a positive relationship with Pd in the

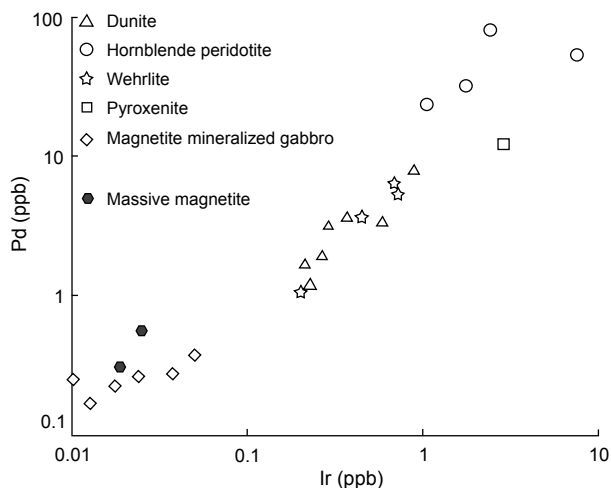


FIGURE 11. Pd-Ir diagram for different lithofacies.

Pobei area (Fig. 11), indicating that the Mss fractional crystallization was weak in Pobei. Therefore, the Pd/Ir values of the Pobei mafic-ultramafic rocks are mainly influenced by the crystallization of silicate minerals. The Pd/Ir values of dunite without sulfide, the lithofacies containing sulfide (including hornblende-peridotite, wehrlite, and pyroxenite) in the Poyi Cu-Ni deposit, magnetite-mineralized gabbro, and massive magnetite ores are 8.19, 12.18, 12.26, and 18.14, respectively. This finding indicates that the massive magnetite was probably the latest product in the evolution of the Pobei mafic-ultramafic intrusions, as the more complete the magma evolution is, the greater is the Pd/Ir.

Based on all the evidence, we think that the magnetite-mineralized gabbro was a late product during crystallization differentiation compared to Pobei

ultramafic rocks, but field evidence shows that the former was emplaced earlier. Hence, the question is, what happened? We infer that the magma differentiation occurred in a deep staging magma chamber. The olivine crystals sank to the bottom of the magma chamber, leaving the less mafic residual magma in the upper part of the chamber (Fig. 12I). At the late stage, the magma became iron enriched through crystallization differentiation. The ultramafic rocks hosting the Poyi and Poshi Cu-Ni sulfide deposits belong to the lower part of the magma chamber, while the magnetite-mineralized gabbro is located in the upper part (Fig. 12I). The magnetite-mineralized gabbro in the upper part of the deep chamber was injected first into the upper chamber (Fig. 12II). The earlier crystallized heavy olivine and some interstitial sulfides were at the bottom of the staging magma chamber and thus were emplaced last (Fig. 12IV), forming the intrusive ultramafic bodies.

CONCLUSIONS

The Cu-Ni sulfide and Fe-Ti oxide ores in the Pobei area were products of a cogenetic parent magma in the Early Permian. The parent magma experienced crystallization differentiation in a deep staging magma chamber. The earlier crystallized olivine and some interstitial sulfides were located at the bottom of the staging magma chamber because they were denser. The magnetite-mineralized gabbro was formed in the upper part of the staging magma chamber at the late stage of the crystallization differentiation process. The magnetite-mineralized gabbro then escaped from the deep staging magma chamber and injected first into the upper magma chamber. Subsequently, the olivine and the interstitial sulfides left the deep staging magma chamber and were finally emplaced in the upper magma chamber.

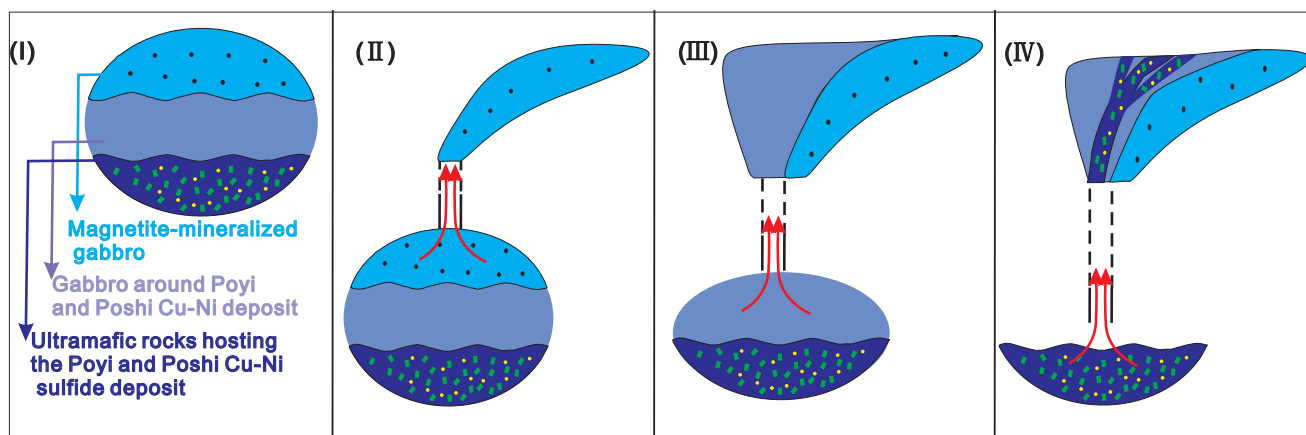


FIGURE 12. Cartoon showing the evolution in the deep staging magma chamber and the emplacement history of the Pobei complex in NW China.

ACKNOWLEDGMENTS

This study was financially supported by the Pobei Cu-Ni Sulfide Deposits Metallogenic Regularity and Location Prediction of Rich Ores of the Xinjiang Province Project (XGMB2012012); the National Science and Technology Support Plan 305 project in Xinjiang (2011BAB06B04-0); the China Geological Survey Projects (DD20160013; 121201011000150005-19); the State Scholarship Fund (201608610016) from the China Scholarship Council; and the China Postdoctoral Science Foundation (2015M582762XB).

REFERENCES

- Adam, J., Green, T., 2006. Trace element partitioning between mica-and amphibole-bearing garnet lherzolite and hydrous basaltic melt: 1. Experimental results and the investigation of controls on partitioning behaviour. *Contributions to Mineralogy and Petrology*, 152(1), 1-17.
- Anderson, A.T., Greenland, L.P., 1969. Phosphorus fractionation diagram as a quantitative indicator of crystallization differentiation of basaltic liquids. *Geochimica et Cosmochimica Acta*, 33(4), 493-505.
- Barnes, S.J., Maier, W., 1999. The fractionation of Ni, Cu and the noble metals in silicate and sulphide liquids. *Geological Association of Canada Short Course Notes*, 13, 69-106.
- Barnes, S.J., Makovicky, E., Makovicky, M., Rosehansen, J., Karupmoller, S., 1997. Partition coefficients for Ni, Cu, Pd, Pt, Rh, and Ir between monosulfide solid solution and sulfide liquid and the formation of compositionally zoned Ni - Cu sulfide bodies by fractional crystallization of sulfide liquid. *Canadian Journal of Earth Sciences*, 34(4), 366-374.
- Bowen, N.L., Schairer, J., 1956. *The evolution of the igneous rocks*. New York, Dover publications, 332pp.
- Bureau of Geology and Mineral Resources of Xinjiang Uygur Autonomous Region (BGMRXUAR), 1993. *Regional Geology of Xinjiang Uygur Autonomous Region* (in Chinese). Beijing, Geological Publishing House, 841pp.
- Capobianco, C.J., Hervig, R.L., Drake, M.J., 1994. Experiments on crystal/liquid partitioning of Ru, Rh and Pd for magnetite and hematite solid solutions crystallized from silicate melt. *Chemical Geology*, 113(1), 23-43.
- Cawthorn, R., Molyneux, T., 1986. Vanadiferous magnetite deposits of the Bushveld complex. *Mineral deposits of Southern Africa*. Johannesburg, Geological Society of South Africa, 1251-1266.
- Chai, F., Zhang, Z., Mao, J., Dong, L., Zhang, Z., Wu, H., 2008. Geology, petrology and geochemistry of the Baishiquan Ni-Cu-bearing mafic-ultramafic intrusions in Xinjiang, NW China: Implications for tectonics and genesis of ores. *Journal of Asian Earth Sciences*, 32(2-4), 218-235.
- Dong, L.H., Cui, B., Qu, X., He, Z.J., Liu, T., Sang, S.J., Wang, W.J., Han, C.M., Bai, G.Y., Guo, H.X., 2005. Location Prediction and evaluation of copper deposits in the middle part of Eastern Tianshan (in Chinese). Bureau of Geology and Mineral Resources and Development of Xinjiang, 268pp.
- Fleet, M.E., Chryssoulis, S.L., Stone, W.E., Weisener, C.G., 1993. Partitioning of platinum-group elements and Au in the Fe-Ni-Cu-S system: experiments on the fractional crystallization of sulfide melt. *Contributions to Mineralogy and Petrology*, 115(1), 36-44.
- Gaetani, G.A., Grove, T.L., 1997. Partitioning of moderately siderophile elements among olivine, silicate melt, and sulfide melt: Constraints on core formation in the Earth and Mars. *Geochimica et Cosmochimica Acta*, 61(9), 1829-1846.
- Griffin, W.L., Pearson, N.J., Belousova, E., Jackson, S.E., Achterbergh, E.V., O'Reilly, S.Y., Shee, S.R., 2000. The Hf isotope composition of cratonic mantle: LAM-MC-ICPMS analysis of zircon megacrysts in kimberlites. *Geochimica et Cosmochimica Acta*, 64(1), 133-147.
- Guo, N.X., Jiang, C.Y., Song, Y.F., Xia, M.Z., Ling, J.L., Xia, Z.D., Wang, B.Y., 2012. Petrogenesis of the Olivine Gabbro-norite in Pobei complex, Northeast Tarim Plate (in Chinese with English abstract). *Geological Review*, 58(5), 873-886.
- Han, B., Ji, J., Song, B., Chen, L., Li, Z., 2004. SHRIMP zircon U-Pb ages of Kalatongke No. 1 and Huangshandong Cu-Ni-bearing mafic-ultramafic complexes, North Xinjiang, and geological implications (in Chinese with English abstract). *Chinese Science Bulletin*, 49(22), 2424-2429.
- Han, C., Xiao, W., Zhao, G., Ao, S., Zhang, J., Qu, W., Du, A., 2010. In-situ U-Pb, Hf and Re-Os isotopic analyses of the Xiangshan Ni-Cu-Co deposit in Eastern Tianshan (Xinjiang), Central Asia Orogenic Belt: constraints on the timing and genesis of the mineralization. *Lithos*, 120(3), 547-562.
- Han, C., Xiao, W., Zhao, G., Benxun, S.U., Songjian, A.O., Zhang, J., Wan, B., 2013. Age and tectonic setting of magmatic sulfide Cu-Ni mineralization in the Eastern Tianshan Orogenic Belt, Xinjiang, Central Asia. *Journal of Geosciences*, 58(3), 233-250.
- He, Z.Y., Sun, L.X., Mao, L.J., Zong, K.Q., Zhang, Z.M., 2015. Zircon U-Pb and Hf isotopic study of gneiss and granodiorite from the southern Beishan orogenic collage: Mesoproterozoic magmatism and crustal growth (in Chinese with English abstract). *Chinese Science Bulletin*, 60(4), 389-399.
- Hill, E., Wood, B.J., Blundy, J.D., 2000. The effect of Ca-Tschermaks component on trace element partitioning between clinopyroxene and silicate melt. *Lithos*, 53(3), 203-215.
- Hirokazu, F., Mitsunobu, T., Ken-Ichiro, A., 1984. Partition coefficients of Hf, Zr, and REE between phenocrysts and groundmasses. *Journal of Geophysical Research Solid Earth*, 89(S02), B662-B672.
- Hu, Z., Gao, S., Liu, Y., Hu, S., Chen, H., Yuan, H., 2008. Signal enhancement in laser ablation ICP-MS by addition of nitrogen in the central channel gas. *Journal of Analytical Atomic Spectrometry*, 23(8), 1093-1101.

- Hu, Z., Liu, Y., Gao, S., Liu, W., Zhang, W., Tong, X., Lin, L., Zong, K., Li, M., Chen, H., 2012a. Improved in situ Hf isotope ratio analysis of zircon using newly designed X skimmer cone and jet sample cone in combination with the addition of nitrogen by laser ablation multiple collector ICP-MS. *Journal of Analytical Atomic Spectrometry*, 27(9), 1391-1399.
- Hu, Z., Liu, Y., Gao, S., Xiao, S., Zhao, L., Günther, D., Li, M., Zhang, W., Zong, K., 2012b. A “wire” signal smoothing device for laser ablation inductively coupled plasma mass spectrometry analysis. *Spectrochimica Acta Part B: Atomic Spectroscopy*, 78, 50-57.
- Jia, C., 1997. Tectonic Characteristics and Oil-gas, Tarim Basin (in Chinese). Beijing, Petroleum Industry Press, 438pp.
- Jiang, C., 2014. Study on Origin of Xiangshan Copper Nickel Sulfide-Ni-Fe Oxide Deposits Petrogenesis and Mineralization of Xiangshan in Eastern Tianshan (in Chinese with English abstract). Dissertation for the Degree of Master. Xi'an (China), Chang'an University, 1-26.
- Jiang, C., Cheng, S., Ye, S., Xia, M., Jiang, H., Dai, Y., 2006. Litho geochemistry and petrogenesis of Zhongposhanbei maric rock body, at Beishan region, Xinjiang (in Chinese with English abstract). *Acta Petrologica Sinica*, 22(1), 115-126.
- Jiang, C.Y., Xia, M.Z., Yu, X., Lu, D.X., Wei, W., Yang, S.F., 2007. Liuyuan trachybasalt belt in the Northeastern Tarim Plate: products of asthenosphere mantle decompressional melting (in Chinese with English abstract). *Acta Petrologica Sinica*, 23(7), 1765-1778.
- Jiang, C.Y., Xia, M.Z., Guo, N.X., Ling, J.L., 2010. geological comprehensive study of Cu-Ni deposit in Pobei area, Xinjiang (in Chinese). Chang'an University, 1-106.
- Jiang, C.Y., Guo, N.X., Xia, M.Z., Ling, J.L., Guo, F.F., Deng, X.Q., Jiang, H.B., Fang, Y.Z., 2012. Petrogenesis of the Poyi mafic-ultramafic layered intrusion, NE Tarim Plate (in Chinese with English abstract). *Acta Petrologica Sinica*, 28(7), 2209-2223.
- Jones, R.H., Layne, G.D., 1997. Minor and trace element partitioning between pyroxene and melt in rapidly cooled chondrules. *American Mineralogist*, 82(5-6), 534-545.
- Kullerud, G., Yund, R.A., Moh, G.H., 1969. Phase relations in the Cu-Fe-S, Cu-Ni-S and Fe-Ni-S systems. *Economic Geology*, 4, 323-343.
- Li, C.N., Lu, F.X., Chen, M.H., 2001. Research on petrology of the Wajilitag complex body in North edge in the Talimu Basin (in Chinese with English abstract). *Xinjiang Geology*, 19, 38-42.
- Li, Z., Zhang, Z.C., Wang, F.S., Hao, Y.L., Ai, Y., Yang, T.Z., 2006a. Open-system magma chamber: an example from the Xinjie mafic-ultramafic layered intrusion in Panxi region, SW China (in Chinese with English abstract). *Acta Petrologica Sinica*, 22(6), 1565-1578.
- Li, Y.C., Zhao, G.C., Qu, W.J., Pan, C.Z., Mao, Q.G., Du, A.D., 2006b. Re-Os isotopic dataing of the Xiangshan deposit, East Tianshan, NW China. *Acta Petrologica Sinica*, 22(1), 245-251.
- Li, H., Chen, F., Mei, Y., Wu, H., Cheng, S., Yang, J., Dai, Y., 2006c. Isotopic ages of No. 1 intrusive body in Pobei mafic-ultramafic belt of Xinjiang and their geological significance (in Chinese with English abstract). Beijing, *Mineral Deposits*, 25(4), 463.
- Ling, J.L., 2011. Geochemical Character and Petrogenesis of Luodong Mafic-Ultramafic Layered Intrusion in Beishan Area, Xinjiang, P.R.China (in Chinese with English abstract). Dissertation for the Degree of Master. Xi'an (China), Chang'an University, 1-50.
- Liu, Y.R., 2011. Geological characteristics of mafic and ultramafic intrusions in the Eastern Xinjiang and the enriching mechanism of the metal elements (in Chinese with English abstract). Dissertation for the PhD Degree. China University of Geosciences, unpublished, 1-162.
- Liu, Y.G., 2015. Diagenesis-mineralization of Copper-Nickel deposits and prospecting indicators in Pobei area, Xinjiang (in Chinese with English abstract). Dissertation for the PhD Degree. China University of Geosciences, unpublished, 1-170.
- Liu, Y., Zong, K., Kelemen, P.B., Gao, S., 2008. Geochemistry and magmatic history of eclogites and ultramafic rocks from the Chinese continental scientific drill hole: subduction and ultrahigh-pressure metamorphism of lower crustal cumulates. *Chemical Geology*, 247(1), 133-153.
- Liu, Y., Gao, S., Hu, Z., Gao, C., Zong, K., Wang, D., 2010. Continental and Oceanic Crust Recycling-induced Melt-Peridotite Interactions in the Trans-North China Orogen: U-Pb Dating, Hf Isotopes and Trace Elements in Zircons from Mantle Xenoliths. *Journal of Petrology*, 51(1-2), 537-571.
- Liu, Y.G., Lv, X.B., Yang, L.S., Wang, H.F., Meng, Y.F., Yi, Q., Zhang, B., Wu, J.L., Ma, J., 2015. Metallogeny of the Poyi magmatic Cu-Ni deposit: revelation from the contrast of PGE and olivine composition with other Cu-Ni sulfide deposits in the Early Permian, Xinjiang, China. *Geosciences Journal*, 19(4), 613-620.
- Liu, Y.G., Lü, X.B., Wu, C.M., Hu, X.G., Duan, Z.P., Deng, G., Wang, H., Zhu, X., Zeng, H., Wang, P., 2016. The migration of Tarim plume magma toward the northeast in Early Permian and its significance for the exploration of PGE-Cu-Ni magmatic sulfide deposits in Xinjiang, NW China: As suggested by Sr-Nd-Hf isotopes, sedimentology and geophysical data. *Ore Geology Reviews*, 72, 538-545.
- Lorand, J.P., Luguét, A., Alard, O., 2008. Platinum-group elements: a new set of key tracers for the Earth's interior. *Elements*, 4(4), 247-252.
- Ludwig, K.R., 2003. User's manual for Isoplot 3.00: a geochronological toolkit for Microsoft Excel. Berkely: Berkely Geochronological Center Special Publication, 4(1), 1-71.
- Mao, J.W., Yang, J.M., Qu, W.J., Du, A.D., Wang, Z.L., Han, C.M., 2003. Re-Os Age of Cu-Ni Ores from the Huangshandong Cu-Ni Sulfide Deposit in the East Tianshan Mountains and its Implication for Geodynamic Processes. *Acta Geologica Sinica-English Edition*, 77(2), 220-226.

- Mao, J.W., Pirajno, F., Zhang, Z.H., Chai, F.M., Wu, H., Chen, S.P., Cheng, L.S., Yang, J.M., Zhang, C.Q., 2008. A review of the Cu-Ni sulphide deposits in the Chinese Tianshan and Altay orogens (Xinjiang Autonomous Region, NW China): principal characteristics and ore-forming processes. *Journal of Asian Earth Sciences*, 32(2), 184-203.
- Misra, K.C., Fleet, M.E., 1973. The Chemical Compositions of Synthetic and Natural Pentlandite Assemblages. *Economic Geology*, 68(4), 518-539.
- Misra, K.C., Fleet, M.E., 1974. Chemical Composition and Stability of Violarite. *Economic Geology*, 69(3), 391-403.
- Nagasawa, H., Schreiber, H.D., Morris, R.V., 1980. Experimental mineral/liquid partition coefficients of the rare earth elements (REE), Sc and Sr for perovskite, spinel and melilite. *Earth & Planetary Science Letters*, 46(3), 431-437.
- Naldrett, A.J., Craig, J.R., Kullerud, G., 1967. The central portion of the Fe-Ni-S system and its bearing on pentlandite exsolution in iron-nickel sulfide ores. *Economic Geology*, 62, 826-847.
- Puchtel, I.S., Humayun, M., 2001. Platinum group element fractionation in a komatiitic basalt lava lake. *Geochimica et Cosmochimica Acta*, 65(17), 2979-2993.
- Qi, L., Zhou, M.F., Wang, C.Y., Sun, M., 2007. Evaluation of a technique for determining Re and PGEs in geological samples by ICP-MS coupled with a modified Carius tube digestion. *Geochemical Journal*, 41(6), 407-414.
- Qin, K.Z., Fang, T.H., Wang, S.L., Zhu, B.Q., Feng, Y.M., Yu, H.F., Xiu, Q.Y., 2002. Plate Tectonics Division, evolution and metallogenic setting in Eastern Tianshan mountains, NW-China (in Chinese with English abstract). *Xinjiang Geology*, 20(4), 302-308.
- Qin, K.Z., Su, B.X., Sakyi, P.A., Tang, D.M., Li, X.H., Sun, H., Xiao, Q.H., Liu, P.P., 2011. SIMS zircon U-Pb geochronology and Sr-Nd isotopes of Ni-Cu-Bearing Mafic-Ultramafic Intrusions in Eastern Tianshan and Beishan in correlation with flood basalts in Tarim Basin (NW China): Constraints on a ca. 280 Ma mantle plume. *American Journal of Science*, 311(3), 237-260.
- Righter, K., Campbell, A., Humayun, M., Hervig, R., 2004. Partitioning of Ru, Rh, Pd, Re, Ir, and Au between Cr-bearing spinel, olivine, pyroxene and silicate melts. *Geochimica et Cosmochimica Acta*, 68(4), 867-880.
- Salters, V.J., Stracke, A., 2004. Composition of the depleted mantle. *Geochemistry, Geophysics, Geosystems*, 5(5), 1-27.
- Scoon, R.N., Mitchell, A.A., 1994. Discordant iron-rich ultramafic pegmatites in the Bushveld complex and their relationship to iron-rich intercumulus and residual liquids. *Journal of Petrology*, 35(4), 881-917.
- Söderlund, U., Patchett, P.J., Vervoort, J.D., Isachsen, C.E., 2004. The ^{176}Lu decay constant determined by Lu-Hf and U-Pb isotope systematics of Precambrian mafic intrusions. *Earth & Planetary Science Letters*, 219(3-4), 311-324.
- Song, X.Y., Zhou, M.F., Tao, Y., Xiao, J.F., 2008. Controls on the metal compositions of magmatic sulfide deposits in the Emeishan large igneous province, SW China. *Chemical Geology*, 253(1), 38-49.
- Song, X., Hu, R., Chen, L., 2009. Geochemical natures of copper, nickel and PGE and their significance for the study of origin and evolution of mantle-derived magmas and magmatic sulfide deposits (in Chinese with English abstract). *Earth Science Frontiers*, 16(4), 287-305.
- Su, B.X., Qin, K.Z., Sakyi, P.A., Liu, P.P., Tang, D.M., Malaviarachchi, S.P., Xiao, Q.H., Sun, H., Dai, Y.C., Yan, H., 2011. Geochemistry and geochronology of acidic rocks in the Beishan region, NW China: petrogenesis and tectonic implications. *Journal of Asian Earth Sciences*, 41(1), 31-43.
- Sun, S.S., McDonough, W.F., 1989. Chemical and isotopic systematics of oceanic basalts: implications for mantle composition and processes. London, Geological Society, 42 (Special Publications), 313-345.
- Tang, D.M., Qin, K.Z., Sun, H., Su, B.X., Xiao, Q.H., 2012. The role of crustal contamination in the formation of Ni-Cu sulfide deposits in Eastern Tianshan, Xinjiang, Northwest China: Evidence from trace element geochemistry, Re-Os, Sr-Nd, zircon Hf-O, and sulfur isotopes. *Journal of Asian Earth Sciences*, 49(3), 145-160.
- Wang, Y., Wang, J., Wang, L., Peng, X., Hui, W., Qin, Q., 2006. A intermediate type of Cu-Ni sulfide and V-Ti magnetite deposit: Xiangshanxi deposit, Hami, Xinjiang, China (in Chinese with English abstract). *Acta Geologica Sinica*, 80(1), 61-73.
- Wang, Y.W., Wang, J.B., Wang, L.J., Long, L.L., 2009. Characteristics of two mafic-ultramafic rock series in the Xiangshan Cu-Ni(V) Ti-Fe ore district, Xinjiang (in Chinese with English abstract). *Acta Petrologica Sinica*, 25(4), 888-900.
- Wang, Y.W., Wang, J.B., Wang, L.J., Long, L.L., Tang, P.Z., 2010. Petrographical and lithochemical characteristics of the mafic-ultramafic complex related to CuNi-VTiFe composite mineralization: Taking the North Xinjiang as an example (in Chinese with English abstract). *Acta Petrologica Sinica* 26(2), 401-412.
- Wiedenbeck, M., Alle, P., Corfu, F., Griffin, W., Meier, M., Oberli, F., Quadt, A.V., Roddick, J., Spiegel, W., 1995. Three natural zircon standards for U-Th-Pb, Lu-Hf, trace element and REE analyses. *Geostandards newsletter*, 19(1), 1-23.
- Wu, H., Li, H., Mo, X., Chen, F., Lu, Y., Mei, Y., Deng, G., 2005. Age of the Baishiqun mafic-ultramafic complex, Hami, Xinjiang and its geological significance (in Chinese with English abstract). *Acta Petrologica Sinica*, Chinese edition, 79(4), 498.
- Xia, M.Z., 2009. The mafic-ultramafic intrusions in the Huangshan region Eastern Tianshan, Xinjiang: Petrogenesis and Mineralization implication (in Chinese with English abstract). Dissertation for the Ph.D. degree. Xi'an (China), Chang'an University, 1-157.
- Xiao, P.X., 2004. 1:200000 district geological Survey report of BiJiashan, 315pp. (in Chinese).
- Xiao, W.J., Zhang, L.C., Qin, K.Z., Sun, S., Li, J.L., 2004. Paleozoic accretionary and collisional tectonics of the Eastern Tianshan (China): implications for the continental growth of central Asia. *American Journal of Science*, 304(4), 370-395.

- Xiao, Q.H., Qin, K.Z., Tang, D.M., Su, B.X., Sun, H., San, J.Z., Cao, M.J., Hui, W.D., 2010. Xiangshanxi composite Cu-Ni-Ti-Fe deposit belongs to comagmatic evolution product: Evidences from ore microscopy, zircon U-Pb chronology and petrological geochemistry, Hami, Xinjiang, NW China (in Chinese with English abstract). *Acta Petrologica Sinica*, 26(2), 503-522.
- Yang, S.H., 2011. The Permian Pobei mafic-ultramafic intrusion (NE Tarim, NW China) and associated sulfide mineralization. Doctoral Thesis. Pokfulam (Hong Kong), 365pp.
- Yang, S.H., Zhou, M.F., Lightfoot, P.C., Xu, J.F., Wang, C.Y., Jiang, C.Y., Qu, W.J., 2014. Re-Os isotope and platinum-group element geochemistry of the Pobei Ni-Cu sulfide-bearing mafic-ultramafic complex in the northeastern part of the Tarim Craton. *Mineralium Deposita*, 49(3), 381-397.
- Zack, T., Brumm, R., 1999. Ilmenite/liquid partition coefficients of 26 trace elements determined through ilmenite/clinopyroxene partitioning in garnet pyroxene. In: J.J. Gurney (ed.). *Proceedings of the 7th 1998: International Kimberlite Conference*. Cape Town, South Africa, Red Roof Design, 986-988.
- Zhang, C.L., Li, X.H., Li, Z.X., Ye, H.M., Li, C.N., 2008a. A Permian Layered Intrusive complex in the Western Tarim Block, Northwestern China: Product of a Ca. 275-Ma Mantle Plume? *The Journal of Geology*, 116, 269-287.
- Zhang, Z., Mao, J., Du, A., Pirajno, F., Wang, Z., Chai, F., Zhang, Z., Yang, J., 2008b. Re-Os dating of two Cu-Ni sulfide deposits in northern Xinjiang, NW China and its geological significance. *Journal of Asian Earth Sciences*, 32(2), 204-217.
- Zhang, M., Li, C., Fu, P., Hu, P., Ripley, E.M., 2011. The Permian Huangshanxi Cu-Ni deposit in western China: intrusive-extrusive association, ore genesis, and exploration implications. *Mineralium Deposita*, 46(2), 153-170.
- Zhao, Y., Xue, C., Zhao, X., Yang, Y.Q., Ke, J., 2015. Magmatic Cu-Ni sulfide mineralization of the Huangshannan mafic-ultramafic intrusion, Eastern Tianshan, China. *Journal of Asian Earth Sciences*, 105, 155-172.
- Zhong, H., Qi, L., Hu, R.Z., Zhou, M.F., Gou, T.Z., Zhu, W.G., Liu, B.G., Chu, Z.-Y., 2011. Rhenium-osmium isotope and platinum-group elements in the Xinjie layered intrusion, SW China: implications for source mantle composition, mantle evolution, PGE fractionation and mineralization. *Geochimica et Cosmochimica Acta*, 75(6), 1621-1641.
- Zhou, M.F., Michael, L.C., Yang, Z., Li, J., Sun, M., 2004. Geochemistry and petrogenesis of 270 Ma Ni-Cu-(PGE) sulfide-bearing mafic intrusions in the Huangshan district, Eastern Xinjiang, Northwest China: implications for the tectonic evolution of the Central Asian orogenic belt. *Chemical Geology*, 209(3), 233-257.
- Zhu, W.G., Zhong, H., Hu, R.Z., Liu, B.G., He, D.F., Song, X.Y., Deng, H.L., 2010. Platinum-group minerals and tellurides from the PGE-bearing Xinjie layered intrusion in the Emeishan Large Igneous Province, SW China. *Mineralogy and Petrology*, 98(1-4), 167-180.

Manuscript received July 2016;

revision accepted November 2016;

published Online February 2017.

ELECTRONIC APPENDIX I

TABLE I. LA-ICP-MS zircon U-Pb dating data from the magnetite-mineralized gabbro

N°	Pb (Total)	Th	U	Th/U	²⁰⁷ Pb/ ²³⁵ U		²⁰⁶ Pb/ ²³⁸ U		t _{206/238}	
	ppm	ppm	ppm		Ratio	1σ	Ratio	1σ	Age (Ma)	1σ
1	174	644	850	0.757	0.3085	0.0110	0.0440	0.0004	277.8	2.7
2	64	248	331	0.749	0.3246	0.0160	0.0435	0.0005	274.5	3.1
3	74	254	477	0.533	0.3128	0.0118	0.0440	0.0005	277.8	3.1
4	104	361	558	0.647	0.3497	0.0156	0.0442	0.0006	279.0	3.4
5	52	204	262	0.778	0.3415	0.0193	0.0438	0.0007	276.1	4.2
6	194	723	906	0.798	0.3133	0.0109	0.0438	0.0004	276.2	2.7
7	124	443	557	0.796	0.3274	0.0130	0.0438	0.0005	276.4	3.0
8	177	656	887	0.740	0.3083	0.0100	0.0436	0.0004	275.0	2.5
9	43	146	254	0.577	0.3207	0.0220	0.0434	0.0007	274.1	4.2
10	41	143	264	0.541	0.3253	0.0205	0.0441	0.0006	278.4	3.5
11	61	228	278	0.820	0.3092	0.0197	0.0434	0.0006	273.9	3.8
12	51	175	359	0.487	0.3163	0.0202	0.0436	0.0005	275.0	3.2
13	32	112	196	0.571	0.3228	0.0238	0.0436	0.0008	275.2	4.7
14	264	947	1348	0.703	0.3193	0.0135	0.0438	0.0005	276.3	3.0
15	56	206	345	0.596	0.3274	0.0196	0.0438	0.0007	276.2	4.2
16	42	137	297	0.462	0.3111	0.0216	0.0438	0.0006	276.1	3.9

TABLE II. Hf isotopic data of zircons from the magnetite-mineralized gabbro

N°	¹⁷⁶ Hf/ ¹⁷⁷ Hf	1σ	¹⁷⁶ Lu/ ¹⁷⁷ Hf	1σ	¹⁷⁶ Yb/ ¹⁷⁷ Hf	1σ	Age	εHf(t)	1σ	fLu/Hf
	Ratio		Ratio		Ratio		(Ma)			
1	0.282717	0.000013	0.000708	0.000016	0.017262	0.000411	277.8	4	0.68	-0.98
2	0.28275	0.000014	0.001898	0.000002	0.048306	0.000208	274.5	4.9	0.7	-0.94
3	0.282742	0.000012	0.000547	0.000018	0.01321	0.00048	277.8	5	0.66	-0.98
4	0.282753	0.00001	0.000341	0.000003	0.00823	0.000067	279	5.4	0.63	-0.99
5	0.282775	0.000014	0.000705	0.000013	0.018106	0.000355	276.1	6.1	0.71	-0.98
6	0.282763	0.000011	0.000411	0.000008	0.01019	0.000203	276.2	5.7	0.64	-0.99
7	0.282765	0.000011	0.000462	0.000003	0.011378	0.000114	276.4	5.7	0.64	-0.99
8	0.282755	0.000012	0.000631	0.000013	0.015371	0.000316	275	5.3	0.66	-0.98
9	0.282748	0.00001	0.001041	0.000029	0.024978	0.000708	274.1	5	0.63	-0.97
10	0.282766	0.000011	0.000941	0.000024	0.023555	0.0006	278.4	5.7	0.65	-0.97
11	0.282751	0.000012	0.00064	0.000001	0.016318	0.000067	273.9	5.2	0.67	-0.98
12	0.282769	0.000013	0.000893	0.000027	0.021364	0.000678	275	5.8	0.69	-0.97
13	0.282754	0.000011	0.000616	0.000014	0.014838	0.000338	275.2	5.3	0.64	-0.98
14	0.282761	0.000011	0.000526	0.000001	0.013147	0.000066	276.3	5.6	0.65	-0.98
15	0.282732	0.000013	0.000745	0.000013	0.018363	0.000301	276.2	4.5	0.69	-0.98
16	0.282773	0.000012	0.00046	0.000001	0.011254	0.000037	276.1	6	0.67	-0.99

εHf(t) was calculated using the method of Blichert-Toft and Albarède (1998); the ¹⁷⁶Lu decay constant is λ=1.865 × 10⁻¹¹ y⁻¹ (Söderlund *et al.*, 2004)

TABLE III. Major elements and REEs of magnetite-mineralized gabbros

	unit	F-4-1	MD-5	H-5-1	YGL-1-1	XCS-B-4	XCS-B-10	B-Fe2-2	B-Fe2-3	B-Fe2-4	B-23	B-28
SiO ₂	(%)	47.6	51.0	50.8	55.8	51.6	51.3	48.5	51.6	51.7	52.4	49.1
Al ₂ O ₃	(%)	16.55	21.3	17.10	17.80	15.40	15.20	15.55	16.30	17.25	16.55	15.40
Fe ₂ O ₃	(%)	11.56	5.85	9.37	11.12	8.58	8.57	16.26	10.02	10.36	11.68	7.33
SO ₃	(%)	0.03	0.02	0.02	0.03	0.01	0.01	0.05	0.01	0.01	0.26	0.10
Cr ₂ O ₃	(%)	0.04	0.01	0.02	0.02	0.09	0.10	<0.01	0.06	0.05	0.04	0.06
P ₂ O ₅	(%)	0.01	0.56	0.25	0.11	0.16	0.15	1.26	0.14	0.16	0.23	0.07
V ₂ O ₅	(%)	0.07	0.02	0.04	0.04	0.03	0.03	0.03	0.04	0.04	0.03	0.03
CaO	(%)	12.45	10.95	11.50	5.07	8.70	8.63	8.51	10.20	9.90	9.17	12.95
K ₂ O	(%)	0.16	0.43	0.28	1.00	0.52	0.47	0.26	0.20	0.21	1.10	0.24
MgO	(%)	6.67	3.24	6.56	4.24	9.57	10.10	3.88	7.69	6.39	3.20	10.90
MnO	(%)	0.16	0.10	0.15	0.16	0.14	0.14	0.24	0.19	0.19	0.45	0.13
Na ₂ O	(%)	2.36	3.97	2.84	2.89	2.98	2.84	3.58	2.66	2.97	3.60	1.77
TiO ₂	(%)	2.79	0.77	1.37	1.20	1.10	1.06	2.56	1.20	1.28	1.13	0.67
NiO	(%)	0.01	0.01	0.02	0.01	0.06	0.06	<0.01	0.04	0.02	0.01	0.01
LOI	(%)	-0.09	0.30	0.07	0.12	0.94	1.08	-0.50	0.10	0.22	0.30	1.23
La	ppm	1.9	13.9	11.7	31.4	7.3	6.2	21.0	4.5	4.5	18.0	3.8
Ce	ppm	4.5	31.7	25.5	59.4	17.7	15.8	51.3	10.4	9.8	38.9	9.3
Pr	ppm	0.69	4.09	3.52	6.85	2.45	2.14	7.00	1.46	1.31	4.85	1.38
Nd	ppm	3.6	18.2	17.2	27.5	11.5	10.5	34.1	7.2	6.7	21.5	6.9
Sm	ppm	1.16	4.61	3.94	4.77	3.23	2.98	8.38	2.14	1.96	5.26	2.05
Eu	ppm	0.94	1.90	1.49	1.87	1.14	1.02	2.68	1.08	1.19	1.60	0.78
Gd	ppm	1.76	5.10	4.91	4.47	3.71	3.75	9.62	2.78	2.33	5.56	2.68
Tb	ppm	0.30	0.77	0.86	0.73	0.63	0.59	1.41	0.48	0.42	0.95	0.43
Dy	ppm	1.73	4.40	4.73	4.33	3.97	3.82	7.76	2.89	2.70	5.59	2.80
Ho	ppm	0.35	0.87	1.14	0.96	0.79	0.76	1.56	0.61	0.51	1.16	0.58
Er	ppm	1.12	2.43	2.98	2.75	2.30	2.32	4.29	1.87	1.65	3.45	1.70
Tm	ppm	0.15	0.30	0.44	0.43	0.33	0.33	0.52	0.23	0.22	0.50	0.25
Yb	ppm	0.94	1.79	2.51	2.91	2.20	2.15	3.21	1.62	1.52	3.24	1.48
Lu	ppm	0.15	0.25	0.45	0.49	0.34	0.32	0.51	0.25	0.23	0.53	0.21
Y	ppm	9.9	23.6	28.9	26.8	21.6	21.0	41.6	15.8	15.2	31.2	15.4
REE	ppm	29.19	113.91	110.27	175.66	79.2	73.7	194.9	53.3	50.2	142.3	49.7

TABLE IV. PGE contents in the magnetite-mineralized gabbros, massive magnetite ores, and lithofacies related to the Cu-Ni deposit in the Pobei area

N°	Sample	Ir ng/g	Ru ng/g	Rh ng/g	Pt ng/g	Pd ng/g	ΣPGE ng/g	Pd/Ir	Reference
G-1	Magnetite-mineralized gabbro	0.05	0.036	0.023	0.205	0.377	0.69	12.26	This Paper
G-2		0.024	0.015	0.007	0.119	0.259	0.424		
G-3		0.038	0.027	0.021	0.203	0.267	0.556		
G-4		0.018	0.027	0.014	0.136	0.221	0.415		
G-5		0.013	0.032	0.017	0.173	0.165	0.4		
G-6		0.01	0.026	0.013	0.18	0.244	0.474		
Ore-1	Massive magnetite	0.019	0.028	0.013	0.292	0.292	0.644	18.14	This Paper
Ore-2		0.025	0.018	0.01	0.153	0.54	0.746		
PGE-1	Dunite in Poyi Cu-Ni deposit	0.228	0.549	0.176	1.859	1.262	4.074	8.19	Liu <i>et al.</i> , 2015
PGE-2		0.298	0.668	0.264	3.369	3.36	7.959		
PGE-3		0.591	1.011	0.184	4.578	3.582	9.946		
PGE-5		0.917	2.805	0.861	4.921	8.495	17.999		
PGE-6		0.272	0.59	0.162	1.905	2.028	4.957		
PGE-7		0.222	0.577	0.15	1.192	1.785	3.926		
PGE-8		0.385	1.403	0.429	3.565	3.743	9.525		
PGE-9			7.64	16.776	4.376	31.942	50.519		
PGE-10	Hornblende-peridotite	2.506	12.724	4.438	41.901	76.681	138.25	12.18	Liu <i>et al.</i> , 2015
PGE-11		1.774	7.838	2.46	23.874	31.569	67.52		
PGE-12		1.08	5.696	1.982	14.694	23.167	46.62		
PGE-13		0.718	1.372	0.42	5.815	5.14	13.46		
PGE-14	Wehrlite	0.203	0.462	0.155	1.747	1.038	3.61		
PGE-15		0.658	1.225	0.452	3.956	5.69	11.98		
PGE-16		0.442	0.941	0.354	3.201	3.563	8.5		
PGE-17	Pyroxenite	2.861	4.815	0.649	14.463	12.063	34.85		